Open Archive TOULOUSE Archive Ouverte (OATAO)

OATAO is an open access repository that collects the work of Toulouse researchers and makes it freely available over the web where possible.

To link to this article :
URL : http://www.sintef.no/globalassets/project/cdf2014/docs/official_proceedings_cfd2014-redusert-filstr.pdf

Any correspondance concerning this service should be sent to the repository administrator: staff-oatao@listes-diff.inp-toulouse.fr

DROP BREAKUP MODELLING IN TURBULENT FLOWS

Benjamin LALANNE[1,4*]**, Sébastien TANGUY**[2,4]**, Jiří VEJRAZKA**[3]**, Olivier MASBERNAT**[1,4]**, Frédéric RISSO**[2,4]

[1] Laboratoire de Génie Chimique, TOULOUSE

[2] Institut de Mécanique des Fluides de TOULOUSE

[3] Institute of Chemical Process Fundamentals, PRAGUE

[4] Fédération de recherche FERMAT, TOULOUSE

* E-mail: Benjamin.Lalanne@ensiacet.fr

ABSTRACT

This paper deals with drop and bubble break-up modelling in turbulent flows. We consider the case where the drop/bubble slip velocity is smaller than or of the order of the turbulent velocity scales, or when the drop/bubble deformation is mainly caused by the turbulent stress (atomisation is not addressed here).

The deformation of a drop is caused by continuous interactions with turbulent vortices; the drop responds to these interactions by performing shape-oscillations and breaks up when its deformation reaches a critical value. Following these observations, we use a model of forced oscillator that describes the drop deformation dynamics in the flow to predict its break-up probability. Such a model requires a characterization of the shape-oscillation dynamics of the drop. As this dynamics is theoretically known only under restrictive conditions (without gravity, surfactants), CFD two-phase flow simulations, based on the *Level-Set* and *Ghost Fluid* methods, are used to determine the interface dynamics in more complex situations: deformation of a drop in the presence of gravity, bubble-vortex interactions. Results are compared with experimental data.

The perspectives to apply this model to breakup in emulsification processes are also discussed.

Keywords: Bubble and droplet dynamics, DNS, breakup modelling, turbulent flows, emulsions.

NOMENCLATURE

Greek Symbols

ρ Mass density, [kg/m^3].

μ Dynamic viscosity, [Pa.s].

$\hat{\rho}$ Ratio of densities: $\hat{\rho} = \rho_d / \rho_c$, [-].

$\hat{\mu}$ Ratio of viscosities: $\hat{\mu} = \mu_d / \mu_c$, [-].

ω Frequency of oscillation, [rad/s]

β Damping rate of the oscillations, [s^{-1}].

∂u Fluctuation of velocity, [m/s].

σ Surface tension, [N/m].

ϕ Level-Set function, [m].

θ Colatitude angle of spherical coordinates, [rad].

κ Interface curvature, [m^{-1}].

Latin Symbols

d Diameter of the drop or bubble, [m].

D Pipe diameter, [m].

R Radius of the drop or bubble, [m].

t Time, [s].

$\tilde{t}$ Normalized time, [-].

r Radial position in spherical coordinates, [m].

K Constant of the model, [-].

P Pressure, [Pa].

$\boldsymbol{U}$ Velocity, [m/s].

$\boldsymbol{g}$ Acceleration of gravity, [m/s²].

$\boldsymbol{D}$ Rate of deformation tensor, [s^{-1}].

a_2 Amplitude of deformation of harmonic 2, [m].

$\widetilde{a_2}$ Normalized amplitude $\widetilde{a_2} = a_2/d$, [-].

We   Weber number, [-].

Re   Reynolds number, [-].

Bo   Bond number, [-].

F Non-dimensional function, [-].

G Non-dimensional function, [-].

P Legendre polynomial.

V_v Vortex velocity, [m/s].

a Length of large axis of an ellipsoid, [m].

b Length of mean axis of an ellipsoid, [m].

c Length of short axis of an ellipsoid, [m].

d_0 Initial distance, [m].

Sub/superscripts

$\overline{}$ Mean value notation.

c Continuous phase.

d Dispersed phase.

l Number of a mode of oscillation.

crit   Critical value that indicates breakup.

th   Values predicted by a theory.

ASC   Used to characterise rising motion.

OSC   Used to characterise oscillating motion.

∞ Used to characterise a value in steady state.

[ ]   Jump notation at the interface.

INTRODUCTION

In industrial chemical processes, turbulent flows with dispersed deformable media (drops, bubbles) are commonly encountered and a better control of the size of the drops is desired for transport, separation issues, and maximization of interfacial area. Examples include oil industry with problems of separation of oil and water, health and food industry with the need to produce emulsions of very fine droplets in high-pressure homogenizers, nuclear energy industry with pulsed extraction columns for treatment of irradiated nuclear fuel or chemical industry for enhancement of mass transfers in gas-liquid reactors.

In CFD Eulerian codes, population-balance approaches are often used to calculate the drop (or bubble) size distribution. These approaches require closure models for coalescence and breakup phenomena.

The present study focuses on breakup phenomena occurring in turbulent flows. A recent review by Liao and Lucas (2009) has shown that several models have been derived to predict breakup probability, breakup frequency, daughter-drop size distribution after breakup. Most of these existing models use a breakup criterion based on a critical Weber number We_{crit}: it consists in a static force balance between the hydrodynamic forces responsible for deformation (turbulent stresses at the scale of the drop) and the force of surface tension that resists to shape deformations. Performing a comparison of these models, Liao and Lucas have shown that they can predict very different breakup frequencies and daughter drop size distributions when applied to a process that is not the one for which they have been calibrated. The conclusion of their paper is that physical improvements are needed for breakup modelling.

We are currently developing a new approach by modelling the deformation process of a drop in a turbulent flow using a scalar parameter $\widetilde{a_2}$ that describes its deformation. In such an approach, the breakup criterion is based on a critical deformation $\widetilde{a_{2\,crit}}$. This new model calculates the dynamic response of drops that are excited by turbulent fluctuations of the continuous phase. As shown in Galinat *et al.* (2007) or in Maniero *et al.* (2012), it gives better predictions of breakup probability than models based on a We_{crit} when compared to experimental breakup statistics.

Section 1 of this article presents our new approach and the physics on which it is based. Then, predictions of the breakup probability with our new model are compared with experimental statistics on heptane drops in a turbulent pipe flow downstream of a restriction. This section will show that our model requires a description of the drop interface dynamics, which lies on two key-parameters: the frequency of oscillation ω_2 and their damping rate β_2. Nevertheless, these parameters are known only in a limited number of situations: in case of deformations of low amplitudes, in the absence of gravity effects and without surfactants adsorbed at the interfaces.

The objective of the present paper is to show how Direct Numerical Simulations can be used to calculate ω_2 and

β_2 in situations of practical interest. To achieve this goal, two-phase flow simulations using the *Level-Set* method are performed. Section 2 describes the numerical methods.

Then, after validation of the code, three examples of interface dynamics are emphasized in section 3: (a) the study of influence of gravity on ω_2 and β_2 for drops, (b) first results on the effect of surface contamination on the shape-oscillations and (c) the study of the interaction between a rising bubble and a single strong vortex.

Finally, the conclusion will introduce several perspectives of development of this model.

A DYNAMIC MODEL OF DROP DEFORMATION

As example of turbulent flow, let us consider a water pipe flow downstream of a restriction at a Reynolds number of 2100 (based on the orifice diameter), where turbulence is generated after the orifice, like in Galinat *et al.* (2007). Fig. 1 shows experimental pictures of a colored heptane drop travelling through this flow. The velocity field has been measured by PIV. From the results, we calculate a local and instantaneous turbulent Weber number We based on the square of the fluctuating velocity $\partial u^2(d)$ between two points distant of the drop diameter d (taking the maximum of the difference between vertical, transversal and diagonal components): $We = \rho\,\partial u^2(d)d/\sigma$. By averaging $\partial u^2(d)$ in time, we obtain a map of the mean turbulent Weber number $\overline{We} = \rho\,\overline{\partial u^2(d)}d/\sigma$, shown in fig. 1. It has been found that $\overline{We}$ is always one order of magnitude higher than other Weber numbers that characterize the inertial drop deformation due to its mean slip velocity or due to the mean flow deceleration in the flow direction after the orifice, indicating that the turbulent fluctuations are the dominant breakup cause in this flow. Nevertheless, breakup locations do not always correspond to locations of maximum values of $\overline{We}$.
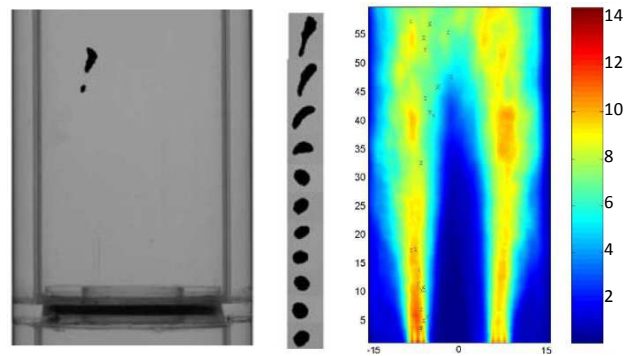
Figure 1: Breakup of a heptane drop downstream of a pipe restriction: deformation of the drop and map of $\overline{We}$ (crosses indicate breakup locations). Figure from Galinat *et al.* (2007).

Fig. 1 illustrates also the deformation process of a drop leading to its breakup. As mentioned by Risso and Fabre (1998), the time evolution of the surface area of the drop shows the existence of a characteristic angular frequency ω_2 which is the frequency of oscillation of its shape. The time scale $t_2 = 2\pi/\omega_2$ is thus characteristic

of the response of an interface submitted to perturbations of its shape, in a similar way to what occurs in turbulent flows.

The problem of the oscillations of a drop submitted to low-amplitude shape deformations has been mathematically studied by Lamb (1932), Miller and Scriven (1968) and Prosperetti (1980). They have theoretically calculated the modes of the oscillations, which are described by means of series of spherical harmonics. A frequency ω_l and a damping rate β_l (due to the dissipation of energy ensured by viscous effects) is associated to the dynamics of each mode of order l. Generally, the mode $l=2$, that represents the oscillation between a prolate and an oblate shape for a drop, is enough to describe the drop or bubble shape in first approximation. Thus, the theoretical expressions given in their papers for ω_2^{th} and β_2^{th} constitute accurate predictions of the characteristic time scales of drop or bubble dynamics.

In order to take into account the interface dynamics in a deformation model, we propose to represent the drop as an oscillator, forced by the turbulent fluctuations experienced by the drop when travelling the flow. If the residence time t_r of the drop in the turbulent field is short compared to its response time t_2, breakup can occur only if the turbulent fluctuations are intense enough, as predicted by a static force balance approach. Nevertheless, if t_r is of same order or larger than t_2, the dynamic response of the drop cannot be ignored. Indeed, in that case, the drop filters the turbulent fluctuations at its own time scale t_2, and its deformation results from a coupling between turbulence and the interface dynamics.

We define a scalar parameter – amplitude of mode 2 of oscillation $\widetilde{a_2}$, normalized by d – to characterize the drop deformation, which is the solution of the following forced oscillator:

$$\frac{d^2\widetilde{a_2}}{d\tilde{t}^2} + 2\frac{\beta_2}{\omega_2}\frac{d\widetilde{a_2}}{d\tilde{t}} + \widetilde{a_2} = K\,We(\tilde{t}) \qquad (1)$$

$\tilde{t} = t/t_2$, and K is a constant parameter of the model that can be identified using experimental data. Breakup occurrence criterion is based on a threshold value of $\widetilde{a_2}$ denoted $\widetilde{a_{2\,crit}}$. Experiments show that the maximum extension of a drop prior to breakup is about twice its diameter, giving an estimation of $\widetilde{a_{2\,crit}} \cong 1/2$, but this value can vary depending on the fluids and the process considered.

Note that a similar approach that describes oscillating and distorting droplets, known as the TAB model (Taylor Analogy Breakup), is commonly used by engineers to calculate breakup in low Weber number sprays (O'Rourke and Amsden (1987)).

The 1D model of eq. (1) requires the knowledge of (i) the time evolution of the turbulent fluctuations $We(\tilde{t})$ experienced by the drop along its trajectory and (ii) the eigenfrequency of oscillation of the drop ω_2 and damping rate β_2. Note that $We(\tilde{t})$ can be obtained

either from PIV measurements (Galinat *et al.* (2007)) or DNS of the single phase carrier flow (Maniero *et al.* (2012)).

As an example, fig. 2 illustrates the computation of the response $\widetilde{a_2}$ of a drop by eq. (1) to a turbulent signal $We(\tilde{t})$ from the experiment of fig. 1. On this signal, $\widetilde{a_2}$ overheads its critical value after 3 periods of oscillation: breakup does not result from a single interaction of the drop with one eddy but from a resonant interaction between the drop and several moderate vortices that allow the drop to accumulate energy of deformation in time. It is clear from this example that a model based on a critical Weber number is not accurate to predict this breakup event. To confirm this, fig. 3 compares the experimental break-up probability to the model (1) predictions for a large number of droplets and using either a critical deformation or a critical Weber number.
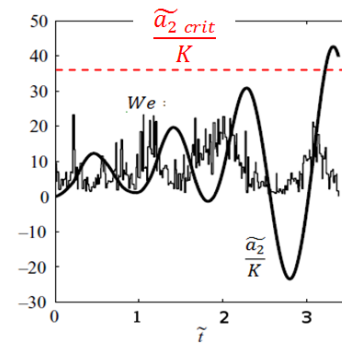
Figure 2: Computation of the deformation of a drop from model (1) using measurements of the turbulence at the scale of the drop We (Galinat *et al.* (2007)).
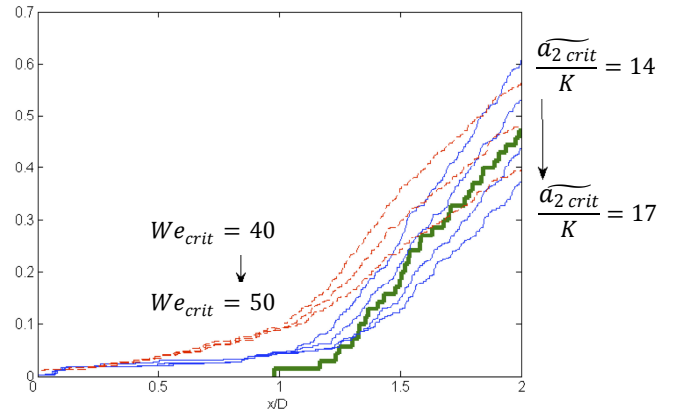
Figure 3: Breakup probability *versus* the distance from the orifice in the pipe. Thick continuous line: experiment. Thin continuous lines: prediction of model (1) assuming different values of $\widetilde{a_{2\,crit}}$. Dotted lines: predictions of model (1) assuming different We_{crit}. Figure from Maniero *et al.* (2012).

It is observed that an approach based on We_{crit} overestimates the breakup probability in the interval $0.5 < x/D < 1.5$ whereas our model based on $\widetilde{a_{2\,crit}}$ well reproduces the experimental data (the best criterion value being $\widetilde{a_{2\,crit}}/K = 16$ for this experiment). That explains why breakup locations do not necessary match with locations of high $\overline{We}$ in fig. 1.

In order to apply our model, one needs to be able to know the times scales $1/\omega_2$ and $1/\beta_2$ describing the

interface dynamics. As already mentioned, theoretical expressions ω_2^{th} and β_2^{th} for these parameters have been derived by several authors; for example, Miller and Scriven (1968) gave

$$\omega_2^{th} = \omega_2^* - \frac{\mu_d}{\rho_d R^2} F \sqrt{Re_d} \qquad (2)$$

$$\beta_2^{th} = \frac{\mu_d}{\rho_d R^2} \left[-2F^2 + G + F\sqrt{Re_d} \right]. \qquad (3)$$

F and G are functions of the density and viscosity ratios given in appendix A, $\boldsymbol{Re_d = \rho_d \omega_2^* R^2 / \mu_d}$, and $\boldsymbol{\omega_2^* = (24\sigma/((3\rho_d + 2\rho_c)\,R^3))^{0.5}}$. Expressions (2) and (3) result from an asymptotic development of the solution at large Reynolds number of oscillation Re_d. They are valid in the linear regime of oscillation (*i.e* for low amplitudes of deformation), disregard the effect of gravity, and are restricted to the case of pure fluids. Thus, it is requested to model the interface dynamics in more complex configurations such as in concentrated emulsions with surfactants. One way to reach this goal is to perform Direct Numerical Simulations in order to include complexity progressively.

Next section describes the numerical methods used in our CFD two-phase flow code.

NUMERICAL METHODS FOR TWO-PHASE FLOW SIMULATIONS

Configurations which are studied in the context of interface dynamics include axisymmetric and three-dimensional simulations of shape-oscillations of rising drops and bubbles, interaction between a bubble and a vortex, and breakup of bubbles/drops in turbulent flows. Direct Numerical Simulations based on the *Level-Set* and *Ghost-Fluid* methods are performed, their outlines are briefly described in this section.

In the *Level-Set* method, the interface is numerically represented by the zero-level curve of a continuous function ϕ which is defined as the algebraic distance to the interface. Its displacement in a velocity field $\boldsymbol{U}$ is computed by solving an advection equation:

$$\frac{\partial \phi}{\partial t} + \boldsymbol{U} . \nabla \phi = 0 \qquad (4)$$

In the framework of a one-fluid approach, the fluid motion is calculated by solving the incompressible Navier-Stokes equations by means of a projection method:

$$\begin{cases} \nabla . \boldsymbol{U} = 0 \\ \\ \dfrac{\partial \boldsymbol{U}}{\partial t} + (\boldsymbol{U}.\nabla)\boldsymbol{U} + \dfrac{\nabla P}{\rho(\phi)} = \dfrac{\nabla . (2\mu(\phi)\boldsymbol{D})}{\rho(\phi)} + \boldsymbol{g} \end{cases} \qquad (5)$$

where P is the pressure, μ the dynamic viscosity, ρ the density, $\boldsymbol{g}$ the acceleration of the gravity and $\boldsymbol{D}$ the rate of deformation tensor. I
n these equations, ρ, μ and P are discontinuous across the interface. The normal stress balance at the interface assumes that

$$[P] = \sigma\kappa + 2\,[\mu\,\partial U_n/\partial n], \qquad (6)$$

where U_n is the velocity normal to the interface, n is the coordinate in the direction normal to the interface, σ the surface tension and κ the interface curvature.

To handle the discontinuity of the pressure at the interface and calculate accurately its derivatives, a *Ghost Fluid method* has been implemented: the jump condition is extrapolated in one ghost cell on each side of the interface. The numerical formulation for the viscous term and the pressure jump at the interface follows the method detailed in Sussman *et al.* (2007).
An algorithm of redistanciation is used to ensure that ϕ remains a distance function at each time step, as described in Tanguy and Berlemont (2005).

These partial differential equations are discretized using the finite volume technique on staggered grids. Spatial derivatives are estimated with a second order central scheme while a fifth order *WENO* scheme is used for the convective terms, which ensures that the solution is robust. Temporal derivatives are approximated with a second-order Runge-Kutta scheme.

DNS OF INTERFACE DYNAMICS

This section illustrates how CFD is used to calculate interface dynamics in several configurations. First, the shape-oscillations of drops and bubbles are calculated and the results used to validate our numerical code. Then, the linear shape-oscillations of rising drops are simulated in order to assess the influence of gravity on the oscillations and to extend the theoretical results in that case. Thirdly, another configuration of interaction between a rising bubble and a single vortex is studied in order to characterise the interface dynamics for non-linear deformations as those occurring in a turbulent flow.

Validation for interface dynamics problems

The numerical methods previously presented are applied to the calculation of shape-oscillations of deformed drops and bubbles. The results obtained are validated against the linear theory of oscillation, or experiments.

Comparison with theory and mesh convergence
Axisymmetric simulations of the shape-oscillations of an initially deformed drop in the absence of gravity are performed. The imposed deformation corresponds to the mode *l*=2 of oscillation with a low initial amplitude $a_2(0)/R = 0.1$. In order to characterise the oscillations, we define a Reynolds number of oscillation, that compares the inertial effects of deformation over the viscous damping: $Re_{OSC} = \rho_C\,(\sigma/(\rho_C R^3))^{1/2}\,R^2/\mu_C$. Three values of Re_{OSC} are investigated: 50, 100, 200. Calculations are performed on a regular mesh of 16, 32 and 64 grid points per drop radius so as to study mesh convergence of the results.

Thanks to the Level-Set function ϕ, the drop contour in spherical coordinates, $r(\theta, t)$ is extracted from the simulation at each time step, and the interface is decomposed into spherical harmonics, reading:

$$r(\theta, t) = R + a_2(t)P_2(\cos\theta), \qquad (7)$$

P_2 being the Legendre polynomial of order l=2.

From the time evolution of a_2, the frequency ω_2 and damping rate β_2 of the oscillations can be obtained and compared against the predictions of the linear theory ω_2^{th} and β_2^{th}:

$$a_2(t) = a_2(0)\cos(\omega_2 t)\, e^{-\beta_2 t}. \qquad (8)$$

	Mesh : N grid points on R	Re_{OSC} = 50	Re_{OSC} = 100	Re_{OSC} = 200
Error on ω_2^{th}	16	-0.07%	-0.51%	-0.43%
	32	0.06%	0.07%	-0.27%
	64	0.19%	0.01%	-0.09%
Error on β_2^{th}	16	0.18%	0.91%	5.67%
	32	-0.68%	-0.45%	-0.07%
	64	-1.15%	-1.07%	-0.76%

Table 1: Validation of the axisymmetric calculation of the shape-oscillations of non-rising drops.

Relative errors are reported in table 1 for the three Re_{OSC}. Results show that the numerical code gives very accurate results on both frequency and damping rates in this range of Re_{OSC}, for grids containing 32 or 64 points in a radius. Spatial convergence of the simulations is also proved by the tests.

Thus, these results provide a good validation of our axisymmetric numerical code to deal with interface dynamics problems. In order to validate also the Cartesian version of the code, a 3D simulation of the shape-oscillations of a bubble is carried out at $Re_{OSC} = 50$ on a grid containing 16 cells in a radius. Results obtained are superimposed on fig. 4 with the curves given by the axisymmetric version of the code with 8, 16, 32 and 64 grid points in a radius.
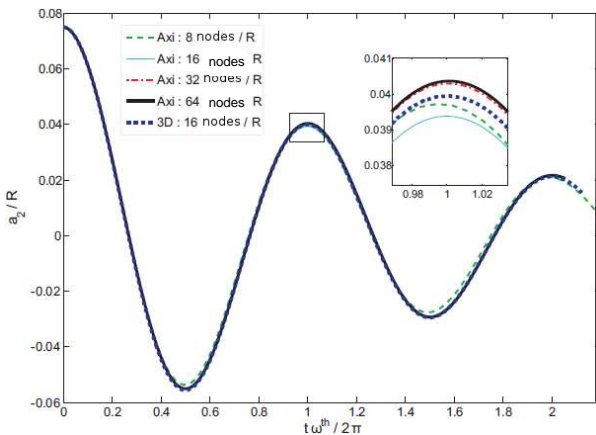
Figure 4: Validation of the 3D Cartesian calculation of the shape-oscillations of a non-rising bubble at $Re_{OSC} = 50$. Figure from Lalanne (2012).

Fig. 4 proves again the mesh convergence of the numerical simulations for the axisymmetric calculations, and shows that the accuracy of the oscillations calculated by the 3D Cartesian version of the code is comparable to that of the axisymmetric calculation with the same number of grid points.

We can then conclude that a calculation with 16 points per bubble radius at $Re_{OSC} = 50$, either in an axisymmetric cylindrical or in a 3D Cartesian domain, gives accurate results in accordance with the theory.

Comparison with an experiment

The code is then validated by comparison with experimental measurements of the shape-oscillations of a slow-rising bubble thanks to a high-speed camera. In the experiment, the bubble is initially attached to a capillary; its sudden translation causes the detachment of the bubble that rises in still water while performing shape-oscillations. The experiment was carried out in ultra-pure conditions in order to avoid contamination due to surfactants. The oscillations, characterized by $Re_{OSC} = 164$, are described using the first ten modes and the initial amplitudes, obtained from the experimental shape at the instant of detachment, are larger than in the previous case ($a_2(0)/R = 0.18$). The Bond number $Bo = (\rho_c - \rho_d)gd^2/\sigma$ is very low ($Bo = 0.08$) to ensure that gravity has negligible effects on both the oscillations and the mean shape of the bubble (which remains spherical during the rising motion).

The shape of the interface is decomposed in spherical harmonics (until order 10):

$$r(\theta, t) = \sum_{l=0}^{10} a_l(t)P_l(\cos\theta). \qquad (9)$$
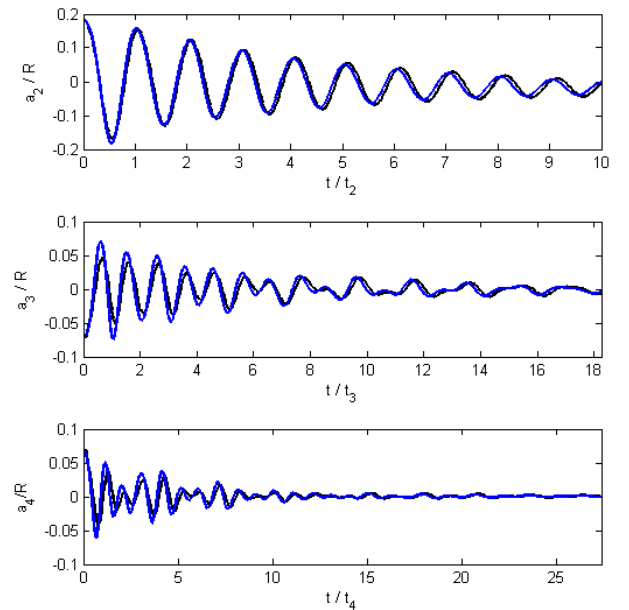
Figure 5: Time evolution of a_2, a_3 and a_4: experiments (black lines) and simulations (blue lines).

Fig. 5 compares the time evolution of a_2, a_3 and a_4 between the experiment and a simulation on a mesh with 32 nodes per bubble radius.

Results show an excellent agreement between the numerical simulations and the experiment for the different modes of oscillation, with a very good accuracy even for strongly damped oscillations (amplitudes less than 0.005R), validating again the use of the present code to capture bubble or drop interface dynamics.

Shape-oscillations of rising drops

We have achieved axisymmetric simulations of a drop rising in a quiescent liquid, its shape being initially elongated in the vertical direction. Thus, while rising, the drop performs shape-oscillations.

The objective is here to understand the effect of the rising motion on the shape-oscillation dynamics, by comparing the frequency and damping rates values with those predicted by the linear theory of oscillation, ω_2^{th} and β_2^{th}, in the absence of gravity.

The problem can be parameterized by four non-dimensional numbers: ratios of density and viscosity $\hat{\rho}$ and $\hat{\mu}$, a Reynolds number of translation $Re_\infty = \rho_C V_\infty d / \mu_C$ based on the rising drop velocity V_∞, and a Reynolds number of oscillation Re_{OSC} based on the oscillating velocity. For these simulations, $\hat{\rho}$=0.99 and $\hat{\mu} = 1$ (liquid-liquid configuration), Re_{OSC} is varied between 50 and 200, and Re_∞ ranges from 60 to 600.

The initial deformation of the drop is set to $a_2/R = 0.1$: it is low enough to ensure a linear regime of oscillation. The regular grid used for the simulation is composed of 32 nodes per drop radius.

Let us examine the shape-oscillations of this rising drop. At $Re_{OSC} = 100$, fig. 6 presents the time evolution of the Reynolds number of rising $Re_{ASC}(t) = \rho_C V(t) d / \mu_C$ for four different values of Re_∞, and fig. 7 displays the corresponding time evolution of the second harmonic amplitude.
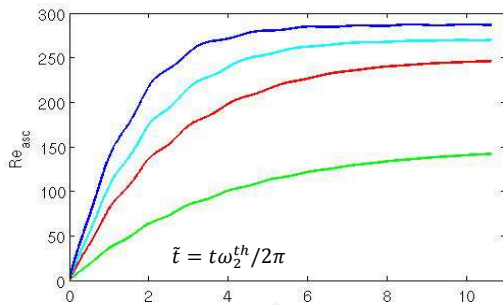

Figure 6: Time evolution of Reynolds number of rising for four drops at $Re_{OSC} = 100$, and $Re_\infty = 150, 200, 270, 290$. Figure from Lalanne (2012).
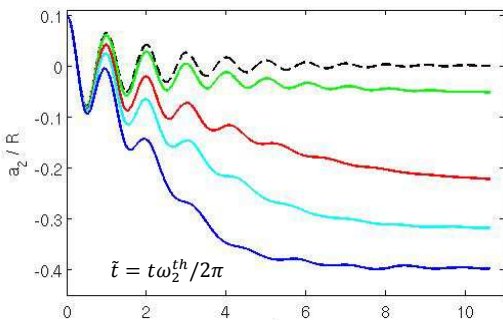
Figure 7: Time evolution of amplitude of harmonic 2 for four rising drops at $Re_{OSC} = 100$, and $Re_\infty = 150, 200, 270, 290$. Dotted line: calculation for a non-rising drop. Figure from Lalanne (2012).

For each drop, the rising velocity increases until the steady state is reached. The translational velocity is very slightly affected by the presence of the shape oscillations. The evolution of the drop shape with time shows that a_2 globally decreases during the acceleration stage since the drop becomes an oblate spheroid due to the rising motion. On this curve, the shape-oscillations due to the initial perturbation are also visible. In order to analyse them and conclude about the effect of the rising motion (*i.e* the effect of Re_∞), we apply a high-pass filter at frequency ω_2^{th} to the time evolution of a_2 in order to separate the evolution of the drop mean shape (which flattens with time) from that of the shape-oscillations. Then, we measure frequency and damping rate of the oscillations on the filtered signal. We observe that the frequency of oscillation is maximum for the non-rising drop and decreases slightly (-10%) when the rising velocity increases. On the contrary, we note a strong increase of the damping rate (until +300%) of the oscillations for the cases at high Re_∞. It is interesting to note that ω_2 and β_2 do not keep constant values for a given set of parameters (Re_{OSC}, Re_∞) but instead they evolve monotonically with time.

This observation leads us to relate the decrease of the eigenfrequency and the increase of the damping rate with the drop instantaneous velocity, which increases with time. Fig. 8 and 9 display the results for drops at $Re_{OSC} = 50, 100, 200$ and several Re_∞: ω_2 and β_2 are presented as a function of an instantaneous Weber number $We(t) = 0.5 (Re_{ASC}(t)/Re_{OSC})^2$ that compares the magnitudes of rising and oscillatory motions. Doing so, time evolutions of both frequency and damping rate seem to collapse on single master curves. Despite a certain scattering of the results that indicates that other factors may play a role on the oscillations (drop acceleration for example), these plots tend to show that the deviation from the theory is mainly controlled by the instantaneous velocity.
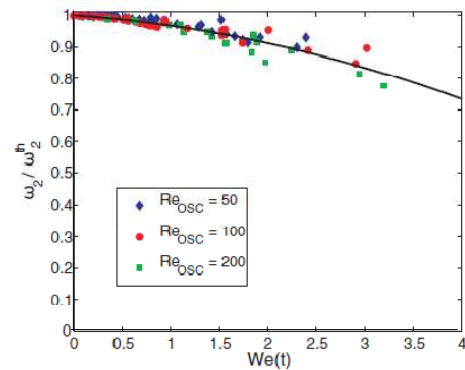
Figure 8: Frequency of oscillation of a rising drop normalized by the theoretical frequency for a non-rising drop, *versus* $We(t)$. Figure from Lalanne *et al.* (2013).

Thus, the main effect of the rising motion on the shape-oscillations of drops is to increase the rate of dissipation of oscillation energy, provided that the rising velocity is large enough compared to the oscillating velocity.

For non-rising drops, the linear theory of oscillation (Miller and Scriven (1968)) shows that the dissipation takes place in boundary layers located on both sides of the interface, as illustrated in fig. 10, which represents the vorticity field of an oscillating drop.
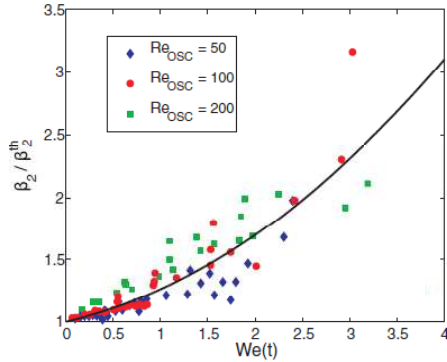
Figure 9: Damping rate of oscillation of a rising drop, normalized by the theoretical damping rate for a non-rising drop, *versus* $We(t)$. Figure from Lalanne *et al.* (2013).

From our numerical simulations, we extract the vorticity field. For slow-rising and oscillating drops, *i.e* when the damping rate of the oscillations is not found to be affected by the translating motion, we observe that the vorticity of the flow is the sum of the vorticity involved in the motion of the same slow-rising drop which does not oscillate (called "pure rising flow"), and of the vorticity involved in the motion of the same oscillating drop that does not rise (called "pure oscillation flow"). Hence, pure rising and pure oscillation flows do not interact in the case of a slow-rising and oscillating drop, explaining why β_2 remains close to β_2^{th}. However, for rapidly rising and oscillating drops, this is not the case: we observe that vorticity contributions of rising and oscillatory motions interact, leading to an increase of the oscillation energy dissipation (*cf* Lalanne *et al.* (2013)).
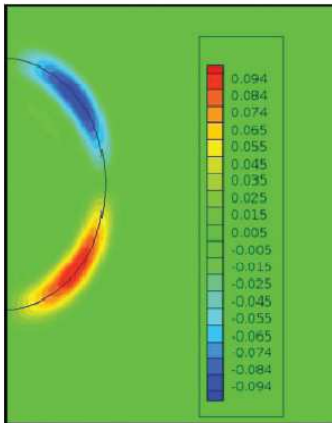
Figure 10: Vorticity field (normalized by ω_2^{th}) of an oscillating and non-rising drop at $Re_{OSC} = 100$. The boundary layers of oscillation visible in this figure are the main location of the dissipation of the energy of oscillation. Figure from Lalanne *et al.* (2013).

Consequently, the effect of the rising motion on the damping rate of oscillation can be explained by looking at the vorticity field during the oscillating motion of the droplets.

For micrometer or millimeter-sized droplets like those commonly involved in many industrial flows, the Weber number based on the rising velocity – as defined here - can hardly be larger than unity. Therefore, the present results (fig. 8 and 9) show that the predictions of the linear theory of oscillation, which do not include the effect of gravity, provide good estimations of ω_2 and β_2 (less than 5% of discrepancy for ω_2 and less than 30% of discrepancy for β_2). This is a practical conclusion, useful to know the limits where the linear theory of oscillation remains valid in order to predict the time scales of the interface dynamics.

Oscillations of contaminated rising drops

Let us consider now the experimental investigation of a shape-oscillating heptane drop which is rising in non ultra-pure water, carried out by Abi Chebel *et al.* (2012). For different drop diameters (millimeter-sized droplets), the authors have measured the damping rates of the oscillations. Results are displayed in table 2 for two contrasted drop diameters. The experimental measurements show that β_2 overestimates by 200% or 300% the theoretical prediction of β_2^{th}, which does not consider either the rising motion or any surface contamination. Using numerical results of fig. 9, we can predict what should be the damping rate of the oscillations in the case of pure fluids and clean interfaces for these rising drops. It is found that the measured damping rates in the experiment are twice these values. Thus, another mechanism is involved: the strong increase of β_2 can be related to the presence of contaminants adsorbed at the liquid-liquid interface. Indeed, it is extremely difficult to carry out experiments with pure fluids in liquid-liquid dispersions. In that experiment, the contamination of the interfaces has been proved by calculating the experimental drag coefficient of the drops, which is found to match that of a solid sphere and not that of a drop with clean interface. We conclude from table 2 that the presence of surface-active contaminants alters significantly the shape-oscillation dynamics. This is probably related to additional tangential stresses that appear close to the interface because of contamination, which may increase strongly the dissipation within the boundary layers of oscillation.

d (mm)	Re_{OSC}	Re_∞	We at steady state	Measured β_2 /β_2^{th}	Prediction of β_2 /β_2^{th} for pure fluids
0.59	120	17	0.01	2.0	1.0
3.52	293	480	1.34	2.7	1.4

Table 2: Experimental results for oscillating and rising heptane drops in non ultra-pure water. From Abi Chebel *et al.* (2012).

Further studies are required to characterise completely the interface dynamics of drops in the presence of surfactants, which depends on the transport properties of these adsorbed contaminants at the interfaces.

Bubble-vortex interaction

In turbulent flows, bubble (or drop) breakup can result from either an interaction with a single intense vortex or with a series of moderate vortices that make the bubble accumulate energy of deformation until breakup (Risso and Fabre (1998)). Therefore, the elementary key mechanism responsible of the deformation of a bubble (or a drop) is its interaction with a vortex. An experimental study of breakup of a rising bubble in a turbulent flow, carried out by Ravelet *et al.* (2011), has shown that large bubble deformations caused by the turbulent fluctuations of the flow are quickly damped, and the authors have not observed shape-oscillations of the bubbles after interaction with strong vortices, contrary to what has been previously reported in microgravity conditions (Risso and Fabre 1998).

In order to investigate this open question of interface dynamics in a turbulent flow in the presence of gravity, three-dimensional simulations of the interaction between a rising bubble and a single vortex have been carried out. The objective of the simulations was to study the response of the bubble after large deformations of its shape.

The non-dimensional parameters that describe the rising bubble are: the ratio of density $\hat{\rho}$=0.001, the ratio of viscosity $\hat{\mu} = 0.016$, the Reynolds number of oscillation Re_{OSC}= 50, the Reynolds number of rising Re_{∞}= 89 or 142. A Hill's vortex of same dimension than the diameter of the bubble has been chosen in order to provoke bubble large scale deformations. Indeed, it is admitted since the pioneering works of Hinze and Kolmogorov that vortices of same size as the bubble diameter are the most efficient for breakup.

The initial condition of the calculation is illustrated in fig. 11. It is the superimposition of the velocity field induced by a Hill's vortex - known analytically, involving a potential flow of characteristic velocity V_{v0}, which is the initial velocity of the Hill's vortex (*cf* Morton (2004)) - and of the flow corresponding to a rising bubble at terminal velocity and characterized by Re_{∞}(calculated through a preliminary simulation). To avoid singular conditions, the vortex and the bubble are off-centered from a distance $d_0 = \sqrt{2}/2 \, R$.

The mesh is Cartesian but non uniform far from the bubble. The bubble dynamics is captured thanks to the use of 16 grid points per bubble radius.

The intensity of the interaction between the vortex and the bubble is scaled by a Weber number based on the velocity V_v of the vortex at the instant it encounters the bubble: $We_v = \rho_C V_v{}^2 \, d/\sigma$.

Fig. 12 displays pictures of the simulation in the case of a very intense interaction: $We_v = 16.5$ and Re_{∞}= 142. Before the interaction, the bubble is flattened with an aspect ratio of 1.84 because of its rising motion. During the interaction, we do not observe bubble breakup but large and non-axisymmetric deformations. To obtain an accurate description of the global shape of the bubble (large scales), we calculate its equivalent ellipsoid.
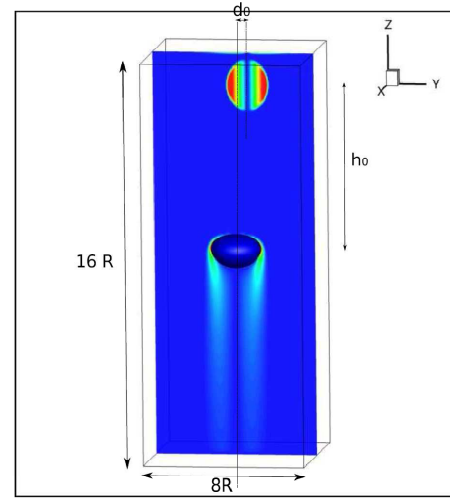
Figure 11: Initial condition (vorticity field) for a 3D-calculation of the interaction of a rising bubble and a Hill's vortex. Figure from Lalanne (2012).

It is defined as the ellipsoid of same inertia matrix as the bubble. In the following, we note a the length of the major semi-axis of the ellipsoid, b the length of the intermediate semi-axis, and c the length of the shorter semi-axis. Fig. 13 displays the evolution of a, b and c in the simulation that corresponds to fig. 12.

The bubble shape is initially symmetric around a vertical axis (see picture 1 of fig. 12) and its rising motion is steady. When the vortex arrives at the bubble location, it causes a large elongation of the bubble and consequently a strong increase of the length of its major axis. In the same time, its medium axis is slightly reduced, leading to a shape close to a cylinder with a large major axis and two small other axes. The maximum deformation can be seen in picture 3 of fig. 12. It is remarkable that the symmetry of the bubble has changed from an axisymmetric oblate shape before the interaction to an axisymmetric prolate shape at the maximum of deformation. Finally, the vortex leaves the bubble, which relaxes towards its equilibrium shape (pictures 4-7 of fig. 12). Its rising motion becomes unsteady and follows a *zig-zag* path.
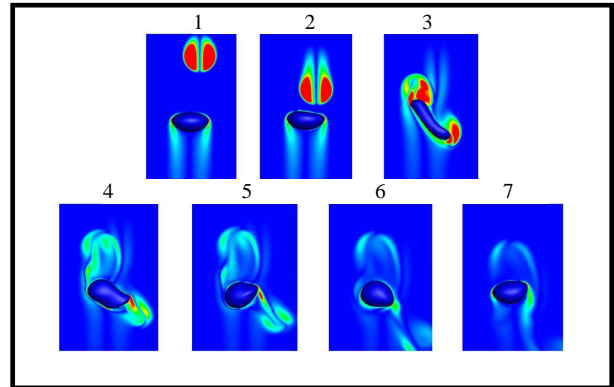
Figure 12: Bubble-vortex interaction at $We_v = 16.5$ and Re_{∞}= 142. Colors correspond to vorticity levels. Time increases with the picture numbers. Note that picture 1 is the initial condition where the bubble has an oblate shape, and picture 3 is that of maximum deformation where the bubble has a prolate shape (close to a cylinder).

It can be observed in fig. 13 that the major part of the large perturbation induced by the vortex is quickly attenuated. The residual departure from the initial shape leads to slowly damped shape oscillations of low amplitudes.

Consequently, the bubble-vortex interaction can be described in two phases: the first one corresponds to a large deformation of the bubble, which is quickly damped; the second one corresponds to the relaxation of the bubble through linear oscillations.
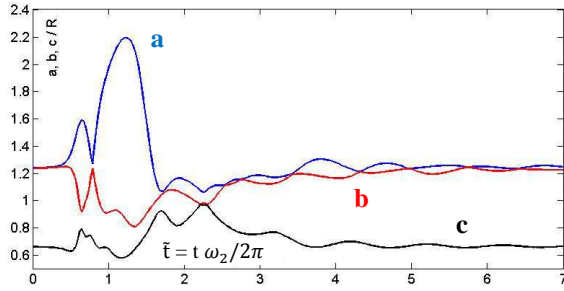
Figure 13: Time evolution of bubble semi-axes during its deformation by a vortex at $We_v = 16.5$ and $Re_\infty = 142$.

Various simulations have been carried out from different sets of parameters (different rising bubble velocities and vortex intensities). The decomposition of the interaction into two phases is relevant for every case.

During the first phase of large deformation, it is observed that the length of the major axis of the bubble is proportional to We_v. Fig. 14 shows the time evolution of the length of the major axis for different cases, the time being normalized by the frequency of oscillation of the rising bubble given by the theory of Meiron (1989). The duration of the large deformation phase is found to be very close to one period of oscillation.

These conclusions are in agreement with the experimental observations of Ravelet *et al.* (2011), who have also noticed that: (1) large deformations correspond to prolate bubble shapes, (2) the duration of the large deformation is equal to one period of oscillation, and (3) statistics of large bubble deformations are proportional to statistics of large turbulent fluctuations.

Hence, in case where the turbulent intensity is weak like in the experiment of Ravelet *et al.* (velocity fluctuations of about 20% of the mean velocity components), the bubble can be considered as a strongly damped oscillator, breakup is rare and occurs only during the interaction with a strong vortex characterized by a large We_v.

Note that, in the simulations, breakup is observed when the bubble elongation (compare to its initial length) is about one diameter, scaling the maximum amplitude a bubble can reach before breaking up.
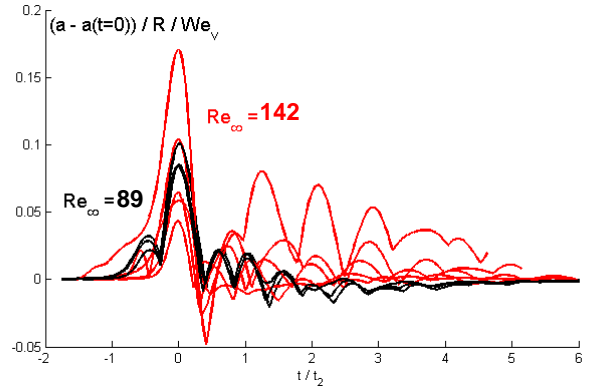
Figure 14: Time evolution the bubble elongation defined as $(a - a(t=0))/R$ and normalized by We_v, for several bubble-vortex interactions at $Re_\infty = 89$ or 142, and $1.5 \leq We_v \leq 16.5$.

CONCLUSION

A new dynamic 1D approach to predict breakup probability of drops or bubbles in turbulent flows has been presented. This approach uses a scalar to describe the dynamics of deformation of a bubble/drop in a turbulent flow and predicts breakup occurrences on the basis of a critical value of deformation, contrary to most of the other existing approaches that consider a critical Weber number. The deformation dynamics is modelled as a linear oscillator forced by the turbulent fluctuations experienced by the particle along its trajectory in the flow. Two time scales are used to characterize the drop-oscillator: its frequency of oscillation ω_2 and the damping rate β_2.

These parameters are theoretically known in limited cases: in the absence of gravity, for low-amplitude oscillations and in the absence of surfactants. The purpose of this paper was to show how CFD simulations (but also complementary experiments) can be used to determine these parameters which are characteristics of the interface dynamics.

In this way, we have studied the influence of gravity on ω_2 and β_2 . For liquid-liquid flows, this influence is generally low due to low density differences. In return, for gas-liquid flows, buoyancy effects have to be accounted for. Hence, simulations of the interaction between a rising bubble and a Hill's vortex reveals overdamped oscillations after a large deformation caused by the vortex. This example of simple configuration is a first step towards a better description of the complexity of breakup phenomenology in turbulent flows, where interactions between a bubble (or a drop) and vortices occur continuously and randomly.

With the aim of handling practical situations like those involved in chemical processes, other effects have to be considered, like those related to the presence of surfactants adsorbed at the interfaces, which provide them additional properties of elasticity and viscosity.

Thanks to comparisons between experimental and numerical measurements of the damping rate of oscillating drops, it has been shown in this paper that the presence of contaminants can modify drastically the interface dynamics. Further studies, combining experimental and numerical tools, are required to tackle more accurately the effect of surfactants on the shape-oscillations dynamics. Moreover, to deal with breakup in concentrated emulsions (e.g. of breakup in high-pressure homogenizers or in static mixers), we should also be able to determine how drop interactions alter the droplet dynamics with respect to the case of an isolated drop, following the work of Galinat et al (2007) where break-up statistics in concentrated emulsions up to 40% have been analysed.

Currently, the proposed model can predict breakup probability of a single drop (with clean interface) travelling in a turbulent inhomogeneous flow.
One objective is to extend this model to turbulent bubbly flows or emulsions with surfactants, after numerical and experimental elementary studies of the interface dynamics.
Another objective is to use the calculated deformation of a drop at the instant of breakup in order to quantify its excess surface energy, and to predict the number and size of daughter drops that will be formed after breakup. We are currently focusing on the validation of such an approach to predict daughter-drop size distribution against experimental data, including cases of binary breakup and breakage into several droplets.
A longer term goal is to develop new breakup kernels that could be implemented in balance population models.

REFERENCES

ABI CHEBEL N., VEJRAZKA J., MASBERNAT O., RISSO F. (2012). Shape oscillation of an oil drop rising in water: Effect of surface contamination. *Journal of Fluid Mechanics*, **702**, 533-542.

GALINAT S., RISSO F., MASBERNAT O., GUIRAUD P. (2007). Dynamics of drop breakup in inhomogeneous turbulence at various volume fractions. *Journal of Fluid Mechanics*, **578**, 85–94.

LALANNE B. (2012) Simulation numérique directe des oscillations, de la déformation et de la rupture d'une bulle en ascension dans un écoulement instationnaire. *Thèse INPT*, Institut de Mécanique des Fluides de Toulouse.

LALANNE B., TANGUY S., RISSO F. (2013). Effect of rising motion on the damped shape oscillations of drops and bubbles. *Physics of Fluids*, **25**, 112107.

LAMB (1932). *Hydrodynamics*. Cambridge University Press.

LIAO, Y., LUCAS, D. (2009). A literature review of theoretical models for drop and bubble breakup in turbulent dispersions. *Chemical Engineering Science*, **64**, 3389-3406.

MANIERO R., MASBERNAT O., CLIMENT E., RISSO F. (2012). Modelling and simulation of inertial drop break-up in a turbulent pipe flow downstream of a restriction. *International Journal of Multiphase Flow*, **42**, 1-8.

MEIRON D.I. (1989). On the stability of gas bubbles rising in an inviscid fluid, *Journal of Fluid Mechanics,* **198**, *101-114.*

MILLER C.A., SCRIVN L.E. (1968). The oscillations of a fluid droplet immersed in another fluid, *Journal of Fluid Mechanics*, **32**, 417-435.

MORTON T. S. (2004). The velocity field within a vortex ring with a large elliptical cross-section, *Journal of Fluid Mechanics,* **503**, *247-271.*

O'ROURKEP. J., AMSDEN A. A. (1987). The TAB method for numerical calculation of spray droplet, SAE Technical Paper, **218**, 872089.

PROSPERETTI A. (1980). Normal mode analysis for the oscillations of a viscous liquid drop in an immiscible liquid. *Journal de Mécanique*, 19, 149-182.

RAVELET F., COLIN C., RISSO F. (2011). On the dynamics and breakup of a bubble immersed in a turbulent flow. *Physics of Fluids*, **23**, 103301.

RISSO F., FABRE J. (1998). Oscillations and breakup of a bubble immersed in a turbulent field. *Journal of Fluid Mechanics*, **372**, 323-355.

SUSSMAN M., SMITH K.M., HUSSAINI M.Y., OHTA M., ZHI-WEI R. (2007) A sharp interface method for incompressible two-phase flows*, Journal of Computational Physics*, **221**, 469-505.

TANGUY S., BERLEMONT A. (2005). Application of a Level-Set method for simulation of droplet collisions. *International Journal of Multiphase Flow*, **31**, 1015-1035.

APPENDIX A

We give here the *F* and *G* functions, associated with eq. (2) and (3), corresponding to the theoretical calculation of Miller and Scriven (1968) for frequency and damping rate of the axisymmetric shape-oscillations of mode $l = 2$, valid for low viscous oscillations of a drop or a bubble (*i.e* at large Reynolds number of oscillation Re_d), in the case of low deformations, in zero-gravity conditions and without surfactants:

$$ F = \frac{25\,(\hat{\rho}\hat{\mu})^{1/2}}{2\sqrt{2}(2\hat{\rho} + 3)(1 + (\hat{\rho}\hat{\mu})^{1/2})} $$

$$ G = \frac{5\,(\,6 + 4\hat{\mu} - \hat{\rho}\hat{\mu} + 16\,\hat{\rho}\hat{\mu}^2\,)}{2\,(2\hat{\rho} + 3)(1 + (\hat{\rho}\hat{\mu})^{1/2})}. $$